The CRM-HL Ecosystem - DLR Contributions

[1]R. Rudnik, [1]S. Pülm, [1]F. Schmidt, [1]J. Wild, [2]A. Schröder, [2]C. Spehr, [1]Ph. Mühlmann

[1]DLR, Institute of Aerodynamics and Flow Technology, 38108 Braunschweig, Germany

[2]DLR, Institute of Aerodynamics and Flow Technology, 37073 Göttingen, Germany

Abstract

With the aim to collect tailored aerodynamic and aero-acoustic data to validate computational fluid dynamics (CFD) methods as well as to improve the understanding of wind tunnel installation effects, DLR carried out experimental investigations of the NASA Common Research Model in high lift configuration (CRM-HL) in the low speed wind tunnel DNW-NWB in Braunschweig. The data are collected and analyzed as part of the DLR project ADaMant. The 5.2% scaled version of the CRM-HL semi span model has been selected as a baseline model configuration. The test campaign is split in two blocks with the first focusing on aerodynamic aspects in the maximum lift regime using the closed test section and the second block utilizing the open test section, which serves to investigate the impact of the test section scenario, but also to carry out aero-acoustic measurements. The aerodynamic tests feature the measurement of forces and moments and static surface pressure data on the model. Transition has been determined on the leading edge devices using infrared thermography. Aerial velocity measurements have been carried out using PIV on selected areas of the flow field of the configurations. The measurements in the open test section have provided forces and moments, as well as pressure distributions over the whole lift regime up to and including $C_{L,max}$. The acoustic properties are determined by microphone arrays and single microphone measurements. Wall array measurements have also been carried out in the closed test section. Next to the original NASA CRM-HL model, a configurative variation with a vented foldable Krueger flap and a UHBR-through flow nacelle with adapted pylon have been investigated in both test sections. An overview of the model modification and selected results of the different measurement techniques is presented.

Keywords: High Lift Aerodynamics, CRM-HL, CFD-Validation, Wind Tunnel Experiments

1. Introduction

Within the framework of the AIAA High Lift Prediction Workshops (HLPW) series, DLR has been continuously contributing with numerical investigations of the NASA High Lift Common Research Model (CRM-HL) [1], [2], [3] since its introduction in HLPW-3 [4]. Based on these experiences and due to the comprehensive numerical and growing experimental data basis, the CRM-HL was selected as the preferred candidate for a dedicated validation experiment as part of the DLR-internal research project ADaMant (Adaptive Data-driven Physical Modeling towards Border of Envelope Applications) [5]. The overall project objective is the improvement of predictive accuracy, efficiency, and usability of the physical modeling in CFD codes with target applications being the borders of the flight envelope. This is accomplished by the enhancement of hybrid RANS/LES methods with a focus on advanced turbulence modeling, scale-resolving simulation approaches, and transition prediction. The enhancements are demonstrated against several dedicated validation experiments, carried out during the project runtime. The CRM-HL represents the most realistic and complex test configuration in ADaMant.

Unlike the other participants in the CRM-HL ecosystem, who are building various scale replicas of

the CRM-HL geometry for testing in their respective wind tunnels, DLR decided to utilize NASA's 5.2% scale semi span model for the ADaMant tests in its original hardware configuration, but at the same time provide and test a configurative variation featuring a larger nacelle with an adapted pylon and a different leading edge device, both designed and fabricated by DLR. For this configuration, designated as DLR CRM-HL, the leading-edge slat of the NASA version is replaced by a vented foldable Bullnose Krueger (VFBK) flap. The standard through-flow nacelle is replaced with an Ultra High Bypass Ratio (UHBR) variant and a corresponding pylon. All DLR components are instrumented, both configurations are depicted in the test section in Figure 1.

After first bi-lateral consultations between DLR and NASA about providing the wind tunnel model for a test in Germany and supporting personnel for model rigging and model handling in early 2020, an implementing arrangement has been set-up between NASA and DLR with the intend to collect unique aerodynamic and aero-acoustic data to validate CFD methods and to improve the understanding of wind tunnel installation effects.

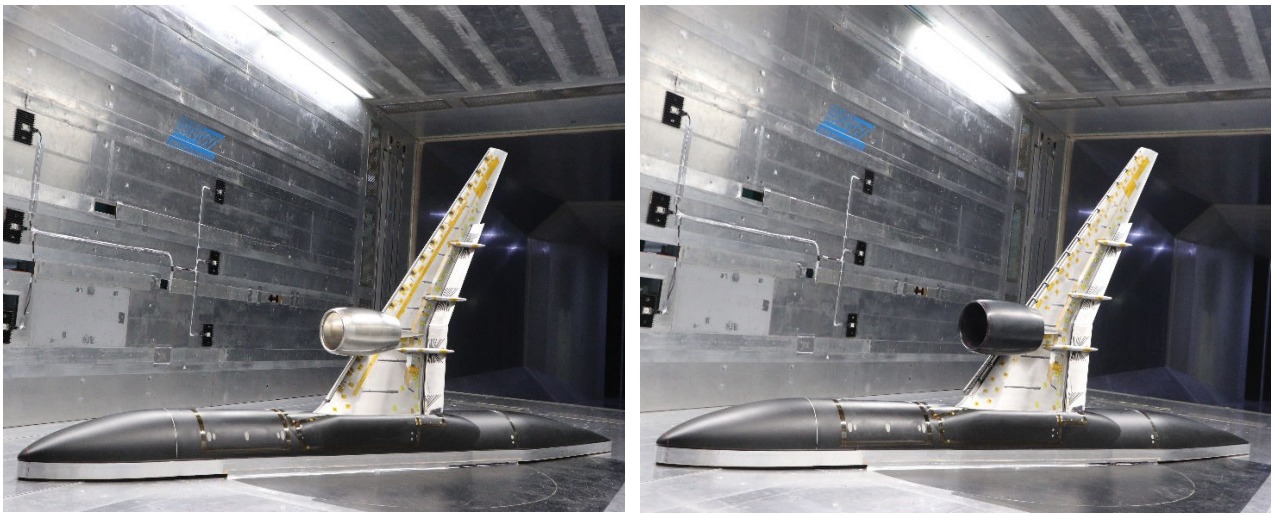

Figure 1 – NASA CRM-HL (left) and DLR CRM-HL (right) in the test section of DNW-NWB.

In order to provide tailored high lift validation data, DNW's low speed facility NWB in Braunschweig, Germany, has been selected. The atmospheric tunnel has a test section of 3.25 m x 2.8 m x 8.0 m. The first tests are focusing on aerodynamic aspects in the maximum lift regime using the closed test section. The second entry utilizes the open test section with floor to investigate the impact of both test section scenarios and to carry out aero-acoustic measurements. The aerodynamic test features measurement of forces and moments, as well as static pressure data on the model surfaces. Transition has been determined on the leading edge devices using Infrared Thermography (IRT). Aerial velocity measurements have been carried out using Particle Image Velocimetry (PIV) on selected areas of the configuration. The aero-acoustic measurement in the open test section have provided forces and moments, as well as pressure distributions over the whole lift regime up to and including $C_{L,max}$. The acoustic properties have been determined by microphone arrays and single microphone measurements. Wall array measurements have also been carried out in the aerodynamic test in the closed test section for the identification of acoustic sources. The rationale and design approach for the model modification are outlined as well as the experimental test set-up. The measurement techniques are briefly described together with selected experimental results.

2. Wind Tunnel Model

2.1 5.2% NASA CRM-HL Model

The NASA CRM-HL model has been designed by Lacy and Sclafani [6] as a low speed full scale configuration based on the high speed wing of the Common Research Model CRM. The first fabricated

wind tunnel model for testing in large low speed facilities like the NASA 14- x 22- foot subsonic tunnel at the Langley Research Center or the QinetiQ 5 Metre wind tunnel was realized as a 10% scaled semi span model. In order to allow high Reynolds number testing in the NASA National Transonic Facility (NTF) or the European Transonic Wind tunnel (ETW), a 5.2% scaled semi span model was designed next, to fit into the respective wind tunnel test sections. This model is fabricated out of VascoMax steel to withstand high pressurized cryogenic test conditions. The configuration consists of a classical swept back wing with a three-element high lift system featuring a leading edge slat and a trailing edge Fowler flap. The overall dimensions of the 5.2% scale model are listed in Table 1. Out of the various device settings, the reference landing setting is selected, as the focus of the investigations described in the present paper is $C_{L,max}$ determination. Slat and flap feature i/b and o/b segments with different device settings [7].

Parameter	Unit	Value
Wing reference area (semi-span)	[m²]	0.51875
Wing reference chord	[m]	0.36428
Wing half-span	[m]	1.52784
Wing quarter choird sweep	[deg]	35
Wing aspect ratio	[-]	9
Wing taper ratio	[-]	0.275
Slat deflection angle IB (Landing)	[deg]	30
Slat deflection angle OB (Landing)	[deg]	30
Flap deflection angle IB (Landing)	[deg]	40
Flap deflection angle OB (Landing)	[deg]	37
Fuselage length	[m]	3.26215

Table 1. Main dimensions and reference landing setting of the 5.2% scale CRM-HL

Compared to the 10% model, minor geometric deviations had to be introduced. This concerns a re-lofting of the trailing edges to allow for the machining of the smaller parts compared to the 10% model. The flap track fairing design has been revised and enlarged to house the pressure tubes routed from the flaps to the main wing spar instrumentation. The i/b flap track fairing is located about 1 track width further inboards compared to the 10% model. The nacelle was re-designed to mitigate separation trends based on lessons learned during tests in the QinetiQ 5 Metre tunnel [8]. The revised nacelle design became the nacelle geometry for the reference CRM-HL model and was used for the nacelle design of the 5.2% model. For the present tests, a stand-off with a total height of 70 mm has been used. More details of the 5.2% model can be found in [9].

2.2 DLR Variant of the 5.2% CRM-HL

One objective of the investigations within AdaMant is to test a variation of the high lift configuration next to the original NASA CRM-HL model. For this purpose, the leading edge high lift system and the nacelle have been replaced [10]. The underlying concept of the modification is to realize exchangeable components for the baseline 5.2% model and to allow arbitrary combinations of the DLR components with those from the original NASA model. Because the original high lift model should not be modified, this concept implies certain design limitations and thus some performance degradations. As the main focus of the model modification remains code validation and not performance optimization, this disadvantage was considered acceptable in certain limits. The design target of the DLR components is the high lift performance of the original CRM-HL at flight Reynolds numbers. Accordingly, the design of the DLR parts has been carried out for full scale flight conditions with the objective to meet the airfield performance requirements of the reference CRM-HL configuration.

For the leading edge, a Vented Foldable Bullnose Krueger (VFBK) has been selected. The Krueger flap has gained renewed attention over the last years as a leading edge device for laminar flow

technology wings. Moreover, according to [11], the rigid Krueger with folding bull nose is cheaper to build and more lightweight than a slat, yet, with a potential performance disadvantage in take-off L/D. It has also been demonstrated that an optimized VFBK can represent an aero-acoustically improved alternative to the slat [12]. As DLR gathered some design expertise for Krueger flaps in European projects like DeSiReH [13] and AFLoNext [14], designing a competitive Krueger flap for the turbulent wing of the CRM-HL appeared to be a technological meaningful challenge. The design of the VFBK is carried out first in 2D for a midboard wing section. The trailing edge flap was not adopted to avoid further model modifications at the trailing edge, despite the fact that a proper alignment of the flap to the leading edge system has some potential to increase maximum lift coefficient of the Krueger-based high lift system. Although being applied to a turbulent wing, the design was guided by shielding considerations and clearance between the main Krueger hinge line and the wing surface, while the size of the Krueger panel is limited by the so-called front-spar clearance addressing system installation aspects. Figure 2 sketches the 2-dimensional Krueger design.

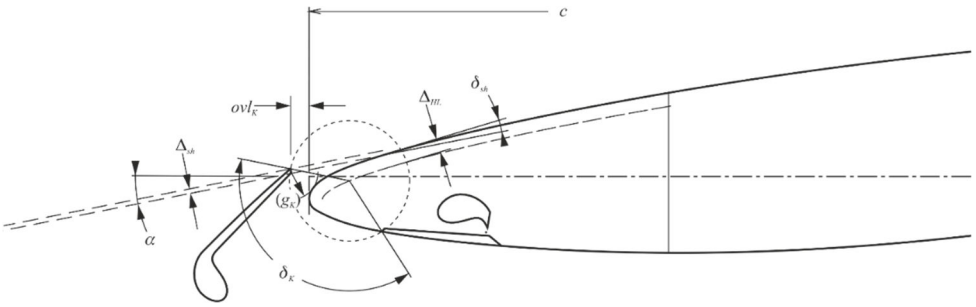

Figure 2 – Section of the VFBK Krueger design [10]

The cavity at the lower side of the clean leading edge for retracting the VFBK and the different track arrangement required the construction and fabrication of a new fixed wing leading edge for the DLR CRM-HL model. A reduction in the Krueger deflection angle for landing at the inboard segment from 130° to 110° is introduced to prevent premature stall on the Krueger close to the engine position.

The Krueger flap is combined with an enlarged nacelle, representative for an ultra high bypass engine. Such concepts represent the next development step for turbofan engines and pose at the same time specific integration challenges in cruise and high lift conditions due to their increased diameter and the resulting close coupling to the wing. The larger secondary mass flow with lower fan pressure ratios allows to improve the propulsive efficiency and leads to lower specific fuel consumption (SFC) of the engine. Moreover, the secondary airflow exits at lower velocities and helps to lower the fan jet noise, accordingly. Thus, the combination of VFBK leading edge and UHBR nacelle in the DLR CRM-HL is a concept that holds promise to be more efficient while having a potential for reduced noise emissions and represents insofar an interesting configurative alternative. Although there are already published studies for the integration of an UHBR engine in combination with the CRM wing geometry, see Ref. [16] and [17], no suitable UHBR through flow nacelle is available. For the present configuration, an approach of a UHBR through flow nacelle designed by DLR for the Airbus XRF-1 nacelle has been adopted [18]. The targeted bypass ratio is 15, which is at the lower end of typical bypass ratios for UHBR engines anticipating to represent the best compromise between propulsive efficiency and installation drag penalties. As these engines are expected to have short nacelles with external mixing to save weight and reduce wetted surfaces, the DLR nacelle is representative for an external mixing layout. It features an axisymmetric core body, which mimics the presence of a core engine to a certain degree. Moreover, it allows to influence the mass flow in certain limits and thus helps to adjust the position of the stagnation line on the nacelle inlet lip. With the core body, the exhaust area is more representative of typical UHBR engines. The initial design of the nacelle was based on the isolated geometry. Then, a pylon was designed using the front section including the crest line to optimize aerodynamic performance in combination with the existing CRM-HL high-lift systems. At the same

time, the pylon nose region has to provide enough space for the model instrumentation while still being representative of a full-scale aircraft.

The contour of nacelle and pylon were optimized by numerical simulations with respect to aerodynamic performance and maximum lift coefficient, specifically to prevent flow separations on the upper outer and lower inner surface. This was achieved by an enlarged nose radius and an increased inlet droop. As for the original NASA nacelle, an inboard strake was added and positioned to delay flow separation on the main wing. For an efficient engine integration, the nacelle is aligned to the local flow in the integrated position. A sketch of the final design is shown in Figure 3.

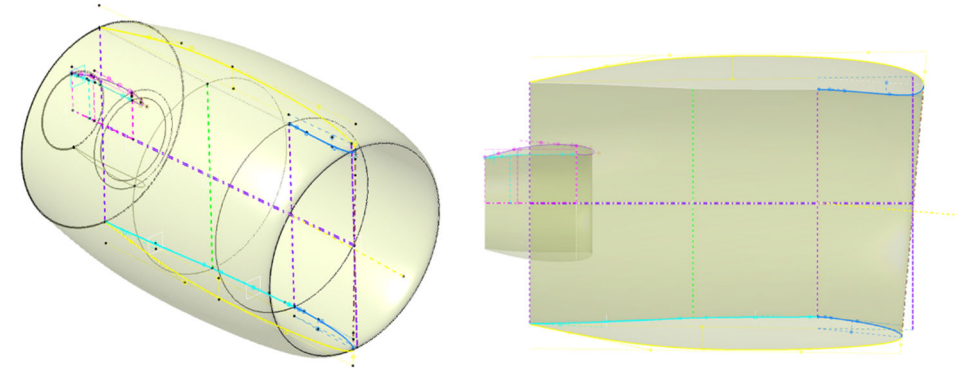

Figure 3 – DLR UHBR through-flow nacelle [10]

The UHBR through-flow nacelle and its pylon have to be designed in such a way that the leading edge high-lift devices of the CRM-HL do not have to be modified in their positioning or have to be cut back in spanwise extension. As a consequence, the spanwise extension is given by the mounting points, and the horizontal nacelle position and the width of the pylon are limited by the inboard and outboard leading edge high-lift devices. The vertical position of the UHBR through flow nacelle is defined by sufficient ground clearance related to the size of the landing gear. The horizontal and vertical position of the nacelle were also varied in the course of the pylon design [10].

The strake orientation as well as its elevation and axial position were optimized in order to delay flow separation on the main wing. Figure 4 shows the integrated nacelle with strake and both high lift devices. More details about the design of the DLR model components can be found in [10].

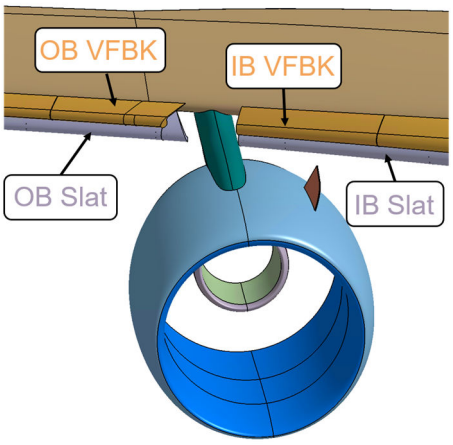

Figure 4 – Integration of the DLR UHBR Through-Flow Nacelle [10]

With the original steel fuselage of the NASA CRM-HL, the overall model weight would have exceeded to limits of the half model balance in the NWB. As the fuselage weight is about twice the weight of the entire high lift wing, it has been decided to re-fabricate the fuselage out of an Ureol block to circumvent

the problem. The black fuselage in Figure 1 is an indicator for the new lightweight fuselage that has been used throughout the tests in NWB. For the atmospheric tests in NWB, the UHBR nacelle has been printed out of ABS, also visible from the black color in Figure 1.

Meanwhile all DLR components have also been fabricated from Inconel, so that also high pressurized cryogenic tests are feasible.

3. Wind Tunnel Testing

3.1 DNW-NWB Facility

The low speed wind tunnel NWB of the German Dutch Wind Tunnels organization DNW is a continuous, atmospheric, low-speed wind tunnel located on the premises of the DLR center in Braunschweig, Germany. It has been refurbished in 2009 and 2010 to add high level aero-acoustic properties to its aerodynamic qualities [19]. NWB is a test facility for commercial and research applications with capabilities for aerodynamic, aero-acoustic, and dynamic testing. Two test section arrangements are available and were used during the ADaMant test campaign. The first test set-up of the ADaMant campaign is linked to the aerodynamic validation activities. It is conducted in the closed test section of 3.25 m x 2.8 m x 8.0 m, typically used for high quality aerodynamic measurements. To account for the boundary layer displacement effect, the tunnel side walls are inclined by 0.2°, while floor and ceiling remain parallel. The closed test section can be operated with slots up to 12% porosity, but this feature has not been utilized during the ADaMant campaign for the sake of simplicity and well-defined boundary conditions for the accompanying numerical validation activities, which are mainly based on in-tunnel simulations. The second test section arrangement is primarily used for aero-acoustic measurements and features an open jet set-up with dimensions of 3.25 m x 2.8 m x 6.0 m. The open test section is surrounded by an anechoic plenum with 99% acoustic damping for a frequency range from 100 Hz to 40 kHz. In order to mount a semi-span model like the CRM-HL, a test section floor is used. This test section configuration is designated as “¾-open”.

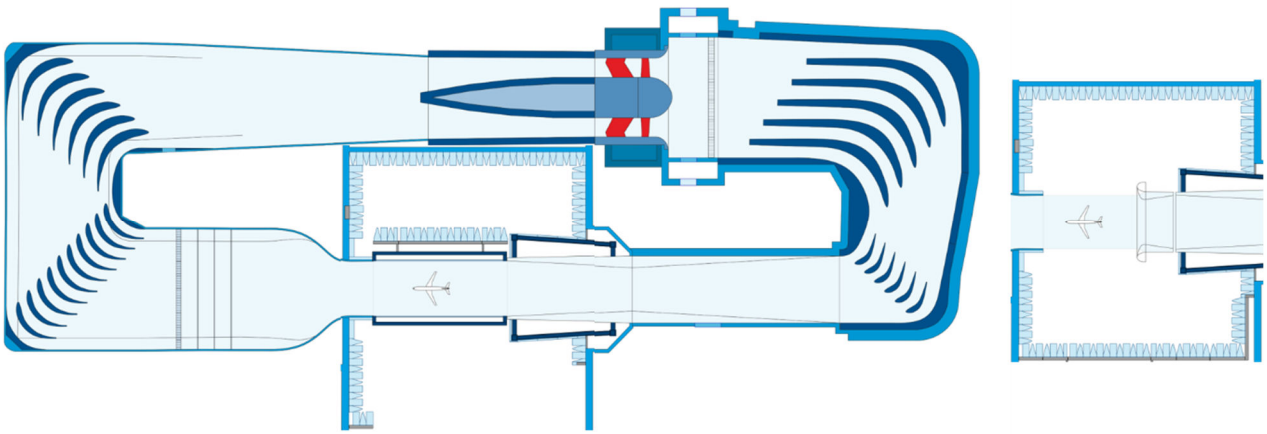

Figure 5 – Schematic of the airline of DNW-NWB and test sections

The wind tunnel can be operated up to 90 m/s, so that Mach numbers up to 0.26 are feasible. The longitudinal turbulence intensity is estimated to 0.06%. The schematic layout of the tunnel with closed section is depicted in Figure 5, the open jet set-up with the anechoic chamber is shown on the right.

Several windows in the walls offer optical access for flow visualization observation or transition measurements with infrared thermography. A custom-made window in the ceiling gives additional optical access from above for flow measurements with PIV. The CRM-HL models in the closed test sections are shown in Figure 1.

3.2 Test Schedule

The test was set-up to conduct measurements with both model variants in both test sections. For selected cases, also mixed component set-ups have been scheduled. Concerning the high lift device setting, the focus has been on the landing configuration in order to provide aerodynamic validation data for $C_{L,max}$ and the lift breakdown. Due to its relevance for aero-acoustic studies, the take-off configuration has been tested as well. In order to determine the influence of the test section set-up on the aerodynamic data and to investigate the impact and limitations of different wind tunnel corrections, as much configuration variants as possible have been tested back to back in both test sections set-ups. A few tests have been carried out with the cruise configuration with and without nacelle in the ¾ open test section.

Taking into account the effort for the change of the test section, the campaign has been split in two blocks, the first being the tests in the closed test section and the second one the tests with the ¾ open test section. Moreover, it has been decided to start with the NASA CRM-HL as it represents an established configuration, which had been already tested shortly before at NASA, and then switch to the DLR variant. The tests campaign lasted from early May to early July 2023. All in all, 28 test days have been devoted to tests in the closed test section and 8 days to those in the ¾ open section.

Concerning flow conditions, the landing configuration has been tested at Mach numbers M = 0.15, 0.2, and 0.23, corresponding to Reynolds numbers of Re = $1.2x10^6$, $1.6x10^6$, and $1.8x10^6$. The angle of attack ranged from α = -10° to 24° using a pitch-pause procedure. The take-off configuration has been tested at Mach numbers of M = 0.20 and 0.23 with the latter being the upper operational limit for the present model. For acoustic testing and infrared detection, a Mach number of M = 0.18 has been added. The average temperature in the test section was measured as 26.7°C with an atmospheric pressure of 1006.3 HPa.

4. Measurement Techniques and Exemplary Results

Basically, the tests covered classical force and moments balance measurements und static pressure distributions in sections of the wing and on the components. The measurements were complemented by flow field measurements using PIV and surface flow visualization based on oil flow and tuft images. Due to the comparatively small Reynolds number, laminar to turbulent transition has been detected by IRT. Acoustic properties of the configuration have been measured by arrays and single microphones in the closed as well as in the ¾ open test section. Exemplary results of the afore mentioned measurement techniques are presented in the following section. More comprehensive presentations and analysis of the test data may be found in Ref.[9], [20], and [21].

4.1 Force and Moment Measurements

Forces and moments have been measured with the floor-mounted six component balance of NWB. The standoff is decoupled by a labyrinth seal from the fuselage. The data have been corrected for wall and tunnel effects following AGARDograph 109.

The comparison between the NASA CRM-HL and the DLR variant for M = 0.2 and Re = 1.6 x 10^6 is depicted in Figure 6. While the lift coefficients and gradients are rather close to each other in the linear lift range, $C_{L,max}$ is lower by about 15 lcts. (1 lct = 0.01) for the variant with Krüger and UHBR. The corresponding angle of attack, α_{max}, is reduced by about 3.5°, accordingly.

This difference has been predicted for low Re No. wind tunnel conditions by numerical analysis throughout the design activity of VFBK and UHBR nacelle [10]. The cross-exchange of both DLR components on the configuration reveals that the lift degradation is basically caused by premature flow separation on the o/b Krueger flap, while the UHBR nacelle tends to improve $C_{L,max}$.

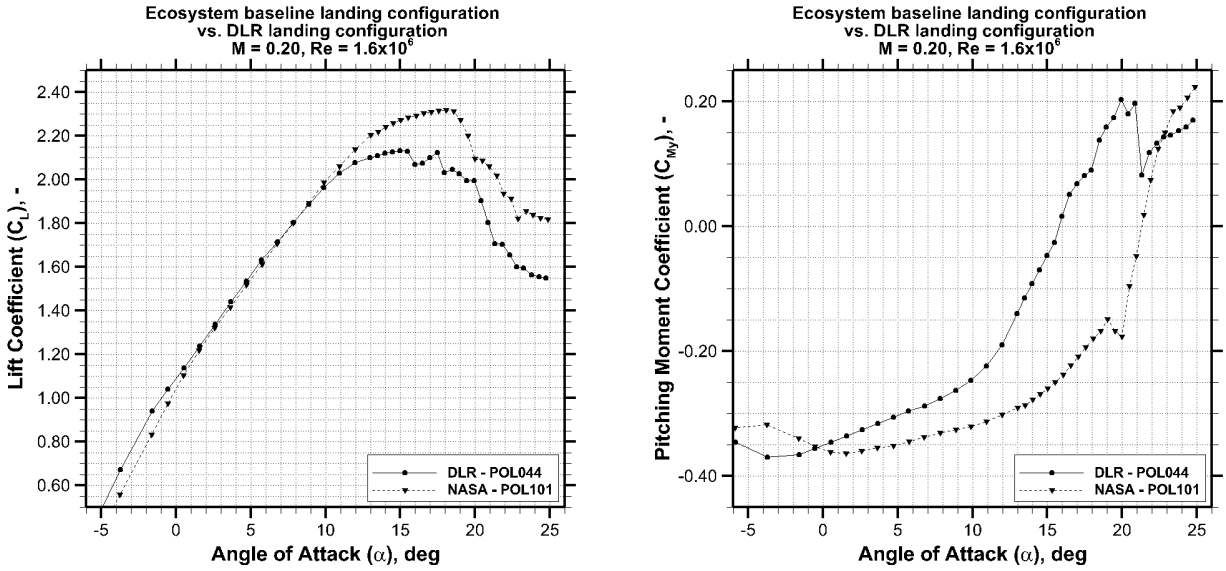

Figure 6 – Lift curve and pitching moment for NASA and DLR configuration at M = 0.20

According to the numerical predictions in [10], $C_{L,max}$ of the DLR variant is at the same level as the reference configuration for full scale design conditions, while $C_{L,max}$ of the VFBK alone slightly exceeds the $C_{L,max}$ level of the slat. Thus, the $C_{L,max}$ degradation of the DLR variant is due to the full scale design philosophy and accepted as such for low Re-No, conditions, as for validation purposes, performance is not the driver, but the challenge to consistently analyze and capture such effects of Re-dependent flow separations consistently. As also can be seen in Figure 6, the nose down pitching moment is considerably reduced for the DLR variant, promising reduced trim efforts.

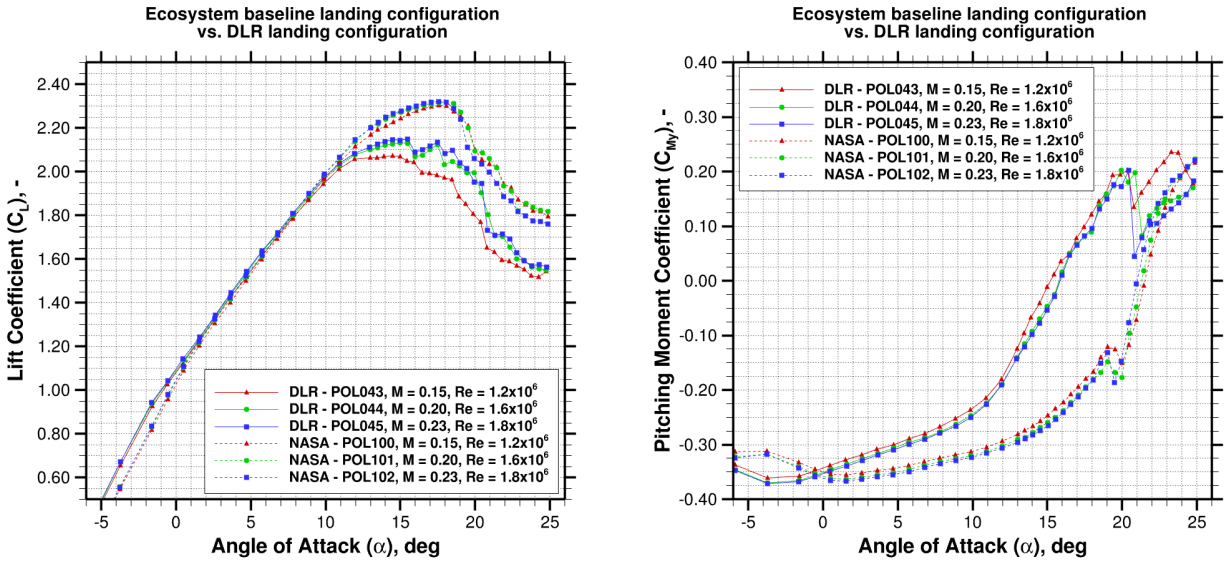

Figure 7 – Lift curve and pitching moment for NASA and DLR configuration and a Mach number variation.

Figure 7 show results for the influence of a combined variation in Mach and Re-No. comprising M = 0.15 and Re = 1.2 x 10^6. M = 0.2 and Re = 1.6 x 10^6, and M = 0.23 and Re = 1.8 x 10^6. As expected, $C_{L,max}$ is increasing with increasing Mach and Re-No. for both configurations, while the linear lift range is hardly affected. The difference from M = 0.15, Re = 1.2 x 10^6 to M = 0.2 to Re = 1.6 x 10^6 is larger than the one between M = 0.2, Re = 1.6 x 10^6 to M = 0.23, Re = 1.8 x 10^6. The increase in $C_{L,max}$ is

largest for the lowest Mach-Re combination and the DLR variant, indicating the flow separation mentioned before is starting to be reduced. The differences in pitching moment are small and similar for both configurations, specifically for the higher combinations. They are widely independent from the angle of attack.

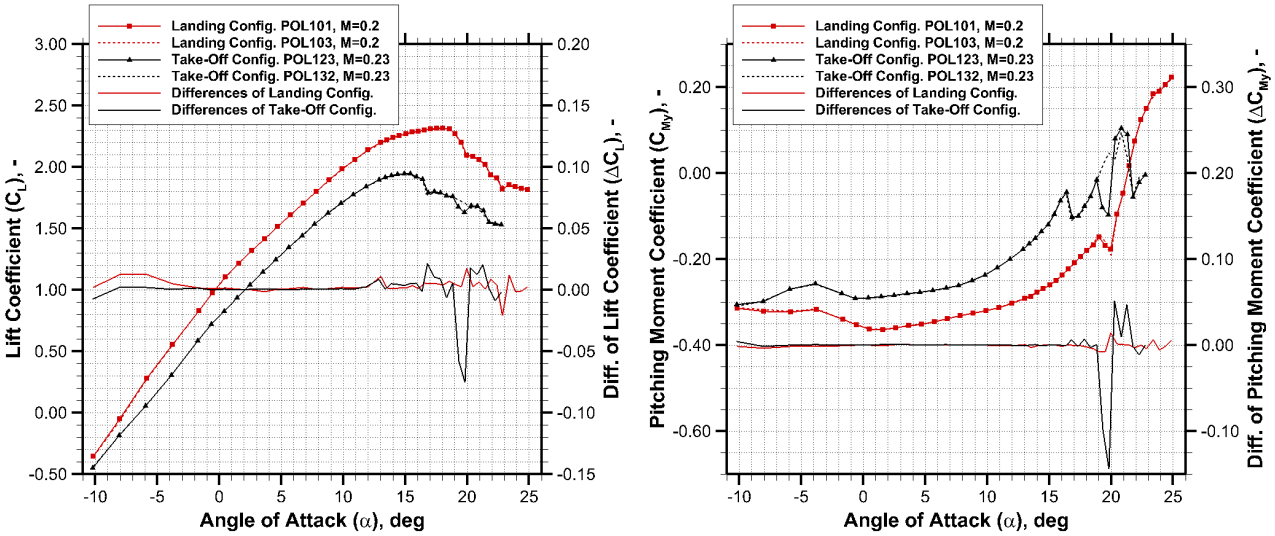

Figure 8 – Lift curve and pitching moment for take-off and landing setting on the NASA CRM-HL

The effect of the high lift device setting is depicted in Figure 8. As expected, the absolute values and the gradient of the lift curve are lower for the take-off setting, defined by 22° slat and 25° flap setting. $C_{L,max}$ is about 15 lcts. smaller in take-off, and the corresponding angle of attack α_{max} about 3.5°. The lift breakdown is as smooth as for the landing configuration. In accordance with the reduced circulation, the nose down pitching moment is considerably smaller for angles of attack up to α_{max}. The force and moment evaluation is also used to assess short term repeatability. The difference between the two polars is small for take-off and landing up to α_{max}, for both, the lift curve and pitching moment. After lift breakdown, larger differences are visible, specifically for the take-off configuration. Global coefficients are also well suited to assess the impact of the test section on the measurements.

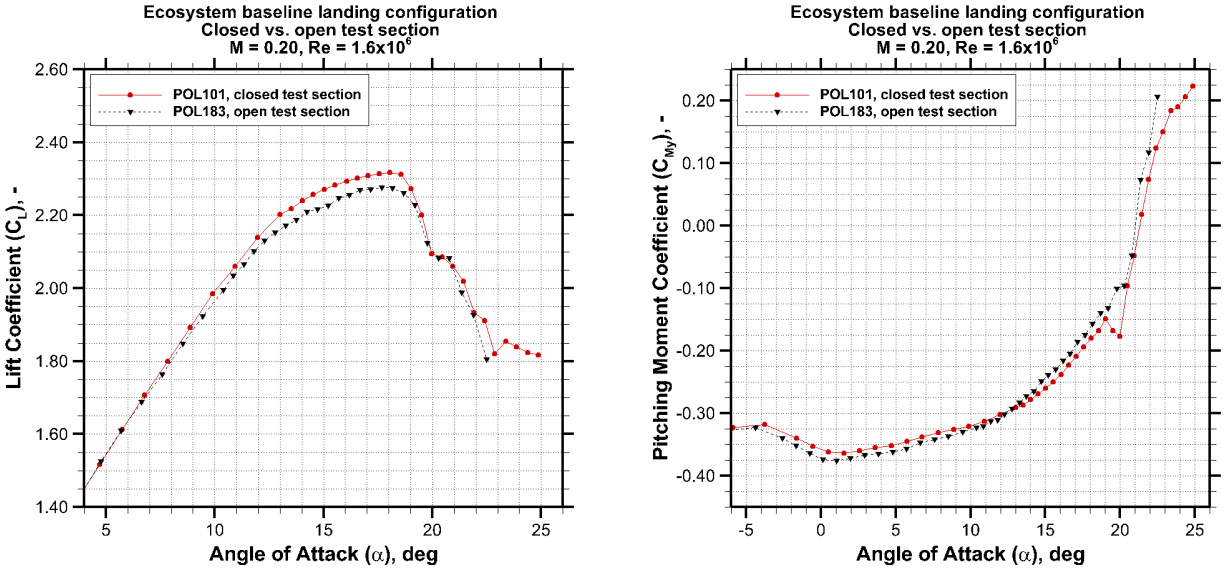

Figure 9 – Lift curve and pitching moment for the NASA configuration in the closed and ¾ open test section

The corresponding results for the lift curve and pitching moment are shown in Figure 9 for the NASA reference configuration. All results are corrected for wall and tunnel effects. The corrected lift curves reveal higher values for the closed test section with deviations starting at about 10° angle of attack. The difference in $C_{L,max}$ amounts to 5 lcts.. Open test sections are oftentimes used for aero-acoustic investigations with a focus on the linear lift range, characteristic for take-off conditions. The deviations in the linear lift range are comparatively small underlining the suitability of open test sections for this purpose. Interestingly, the differences in pitching moments change sign with angle of attack, see right hand side of Figure 9. While the pitching moment measured in the closed test section is less negative in the linear lift range, it is more negative for angles of attack beyond 12°. The amount of differences in pitching moment is widely independent of the incidence and comparatively small.

4.2 Static Pressure Measurements

The pressure measurements have been carried out based on the existing instrumentation with pressure taps of the NASA CRM-HL. There are 179 pressure taps in ten sections on the fixed wing, 55 taps on the slat, 63 on the flap, and 17 taps on the nacelle outer surface. Seven differential pressure scanners with tailored pressure range were installed in the fuselage. The number of pressure taps on the single model components of the DLR model variant matches the one of the reference configuration, with the exception of the outboard Krüger flap, which has 8 taps more than the slat. The distribution of the pressure taps and the location of the pressure sections can be found in [9] and at https://hiliftpw.larc.nasa.gov.

Trends of the lift build-up and breakdown of the NASA reference configuration can be seen in the pressure distribution in row B and H in Figure 10. Note that the outboard section is beyond the spanwise flap extension, so only slat and fixed wing are present. An angle of attack in the linear lift regime (α = 7.8°), at $C_{L,max}$ (α = 18.1°), and after lift breakdown (α = 20°) are analyzed.

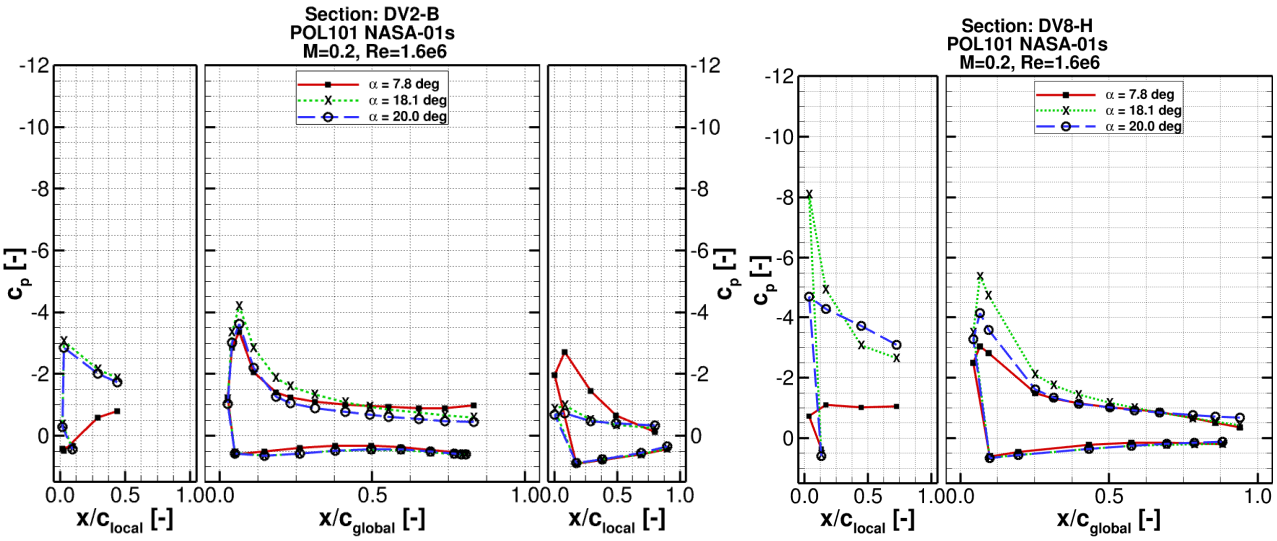

Figure 10 – Pressure distributions B and H for the NASA configuration in the closed test section

When comparing the green and the blue distributions, the lift breakdown in section B is clearly caused by the main wing. The o/b section H also shows this trend together with a collapsing of the slat suction peak. The situation is different for the DLR variant with the Krüger flap, displayed in Figure 11. At section B, the suction level on the leading edge device is still getting stronger corresponding to increasing lift generation when comparing the distributions for α = 18.1° and 19.9°, while there is hardly any difference on the fixed wing, and a slight loss of lift on the trailing edge flap. At the o/b section H, the suction level and the lift generation are continuously decreasing with increasing angle of attack on both elements.

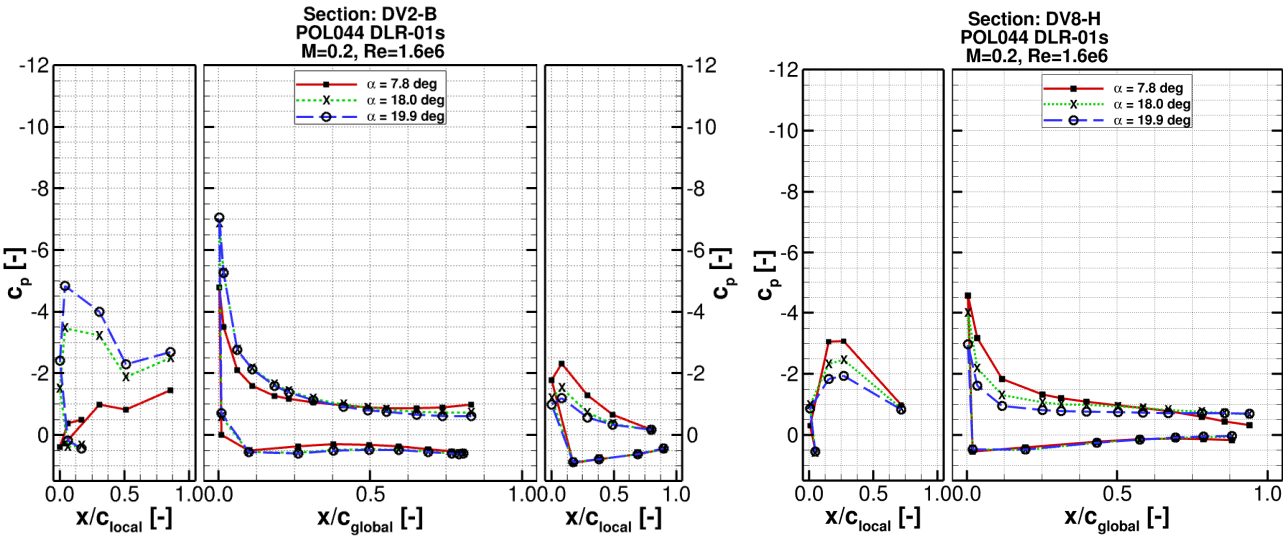

Figure 11 – Pressure distribution B and H for the DLR configuration in the closed test section

The evaluations are still ongoing. A more detailed discussion of the pressure distributions for the DLR variant will be provided in [20].

4.3 PIV Measurements

The PIV team of DLR [22] carried out flow field measurements for both CRM-HL configurations in the closed test section of NWB. For this purpose, the landing setting was investigated for a Mach number of M = 0.2, exclusively. In order to allow statistical evaluations, stereoscopic PIV has been applied taking over 7000 pictures per laser light sheet, camera, and data point. Aerosol seeding has been injected downstream of the test section to achieve a homogenous particle distribution. It was decided to measure planes with longitudinal orientation as can be seen on the left of Figure 12.

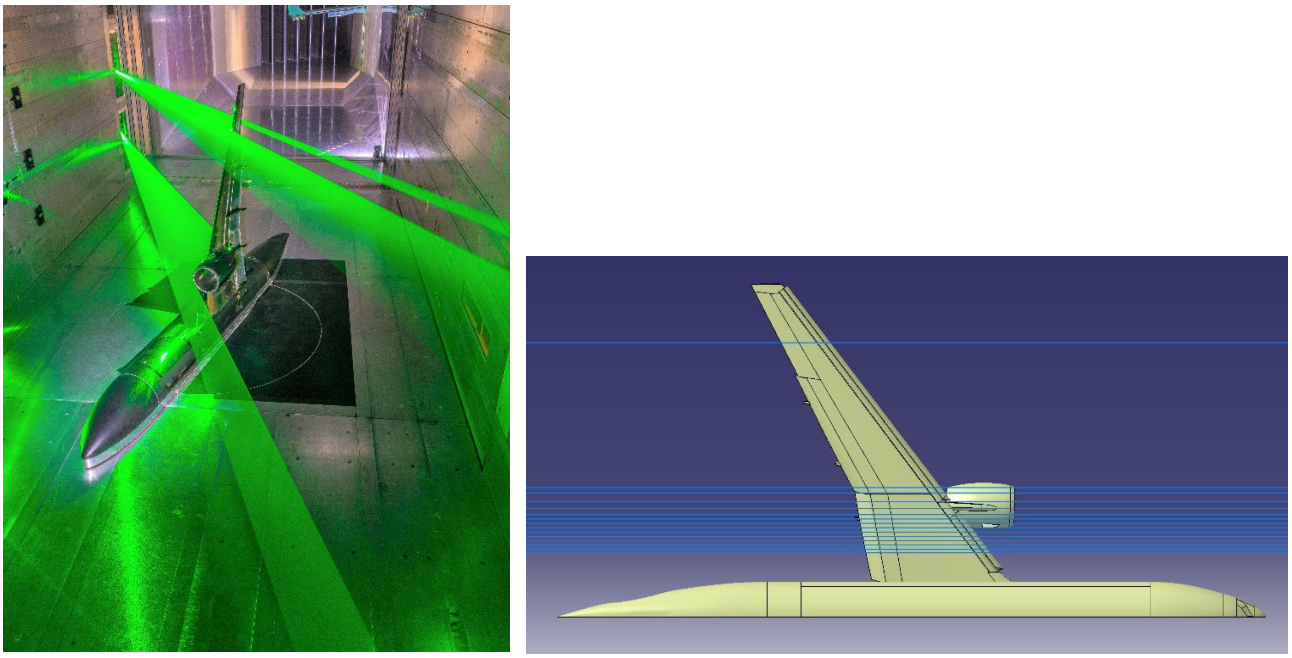

Figure 12 – Laser light sheets in the closed test section and their spanwise positions

14 light sheets were distributed in the vicinity of the nacelle between 19% and 39% half span to observe interference phenomena between nacelle and high lift wing. A single light sheet has been positioned at the outboard wing at about 82% half span to capture flow separation that was expected

there. The locations of the light sheets are displayed on the right side of Figure 12. A total of six PCO.edge cameras were operated using an element of the ceiling wall with windows for optical access, which was specially designed for the present purpose. 4 cameras were observing the inboard wing and 2 the outboard section. The four double-pulse lasers had a frequency 15 Hz at the inboard region and 5 Hz for the outboard section.

As an example, a time-averaged and an instantaneous PIV image taken at 29.2% half span are shown in Figure 13. The confined lower velocity area (green spot) above the leading edge in the time-averaged picture is attributed to the strake vortex passing through the light sheet.

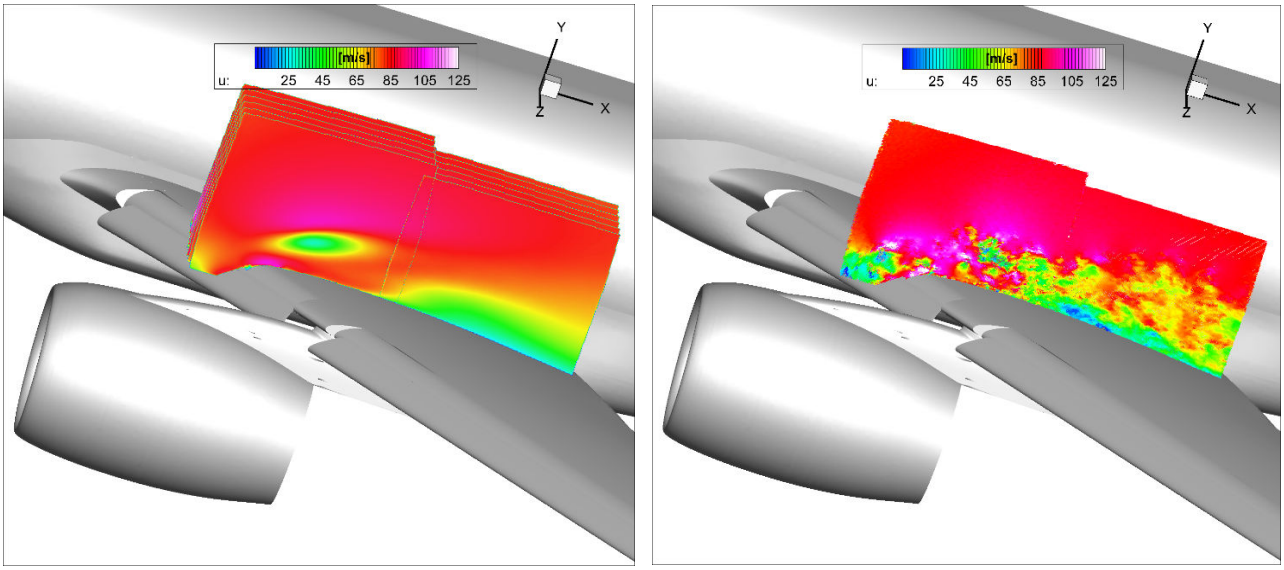

Figure 13 – Time averaged (left) and instantaneous (right) PIV images above the wing for the NASA CRM-HL configuration for M = 0.2 and α = 19°

The instantaneous picture at the same spanwise position on the right exhibits some turbulent structures developing over the wing chord.

4.4 Surface Flow Visualization

Surface flow visualization was carried out using oil flow and tufts in a complementary way. The target area for application was the outboard wing, where preceding experimental and numerical studies [23] have provided evidence for flow separation provoked by an interaction of the wakes of the slat brackets and the fixed wing boundary layer. The model surface has been covered with foil to prevent oil paint from intruding the pressure taps. A special start-up procedure of reaching the desired flow condition was developed [9] to optimize the generation of the oil flow pictures.

Tufts were attached on the same region of the outboard wing, where the oil flow was applied. Moreover, tufts were attached on the upper surface of the inboards wing up to pressure section D and on the upper side of the outer nacelle contour. The recording was accomplished by two cameras mounted outside of the test section looking through the sidewalls on the wing's upper surface.

An example of the oil flow images and tuft visualization is given in Figure 14, taken from [9]. The oil flow image for α = 12.9° in the upper left part shows the wakes of slat track 14 and 15 and their delta-shaped widening towards the fixed wing's trailing edge. These wakes are significantly widening with increasing angle of attack causing substantial loss of lift. This is documented by the image in the lower part of Figure 14 corresponding to an angle of attack of α = 19°, where lift breakdown has started. The separated areas are indicated by red dashed lines. The corresponding tuft photos on the right side of Figure 14 tend to confirm this statement. For better interpretation, the tufts are marked: red straight lines indicate attached tufts, red conical shaped areas agitated tufts, and red strongly curved lines flow

separation. Yet, the tufts fail to reliably describe the area of flow separation, which might be attributed to insufficient spatial resolution.

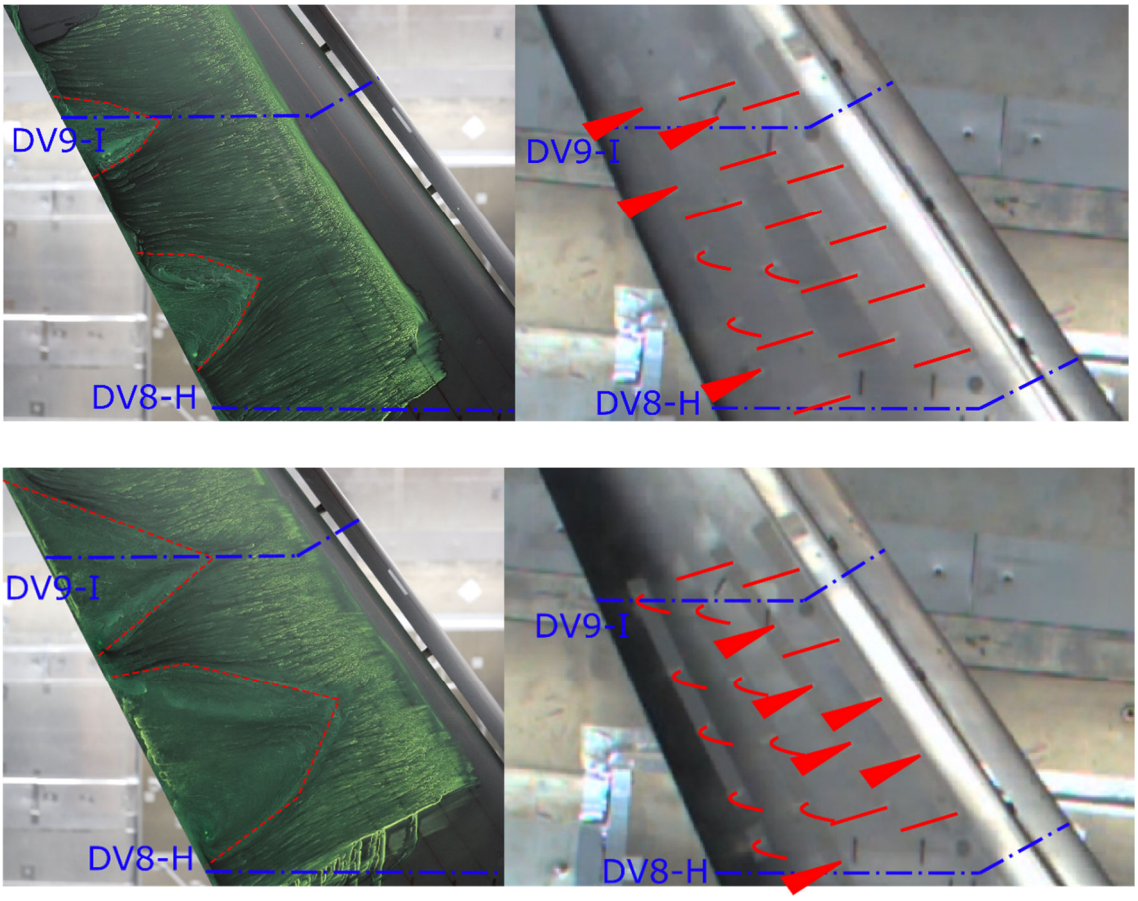

Figure 14 – Surface flow visualization with oil flow and tufts on the outboard wing of the NASA CRM-HL configuration for M = 0.2 and α = 12.9° (upper pictures) and 19° (lower pictures), [9]

A more detailed discussion of the surface flow visualization is provided in Ref. [9].

4.5 Transition Detection

Laminar to turbulent transition has been detected on the leading edge devices by infrared thermography in the closed test section of NWB. For the NASA CRM-HL steel model, an acrylic foil has been applied to the slat surface for thermal insulation in order to reduce the heat flux between model and fluid. For the DLR model variant, a special Krüger flap has been fabricated out of CFRP.

Two FLIR SC3000 cameras and one InfraTec VarioCam HD Head 800 camera have been used to cover the leading and trailing edge part of the midboard wing (Cam 2 and 3) and to outer wing (cam 1). For chordwise orientation, markers have been applied to the wing's upper surface at 10%, 20%, 30%, 40% and 50% local chord. Single pictures as well as video sequences in a later phase of the campaign have been recorded with the latter allowing to observe unsteady transitional effects in certain limits. Measurements have been carried out for both model variants for M = 0.15, 0.18, and 0.20.

Basically, only limited transition fixing by trip dots have been applied to the wing. This concerns the fixed wing at the root inboard of the slat, behind the slat cut-out, and at the wing tip. In addition, tripping has been applied at the fuselage nose and nacelle inlet lip. In order to assess the influence of these tripped areas on the wing, transition detection has been carried out with the trip dots and with removed

trip dots for the NASA CRM-HL. Moreover, test runs with limited tripping on the slat and the Krüger flap between slat tracks 13 and 14 have been conducted. No negative impact of the tripping has been observed. Therefore, the baseline tripping concept as described above has been maintained for the runs with transition detection.

Figure 15 provides an example of the infrared pictures of the three cameras and an angle of attack close to the maximum lift coefficient of the NASA CRM-HL in landing configuration.

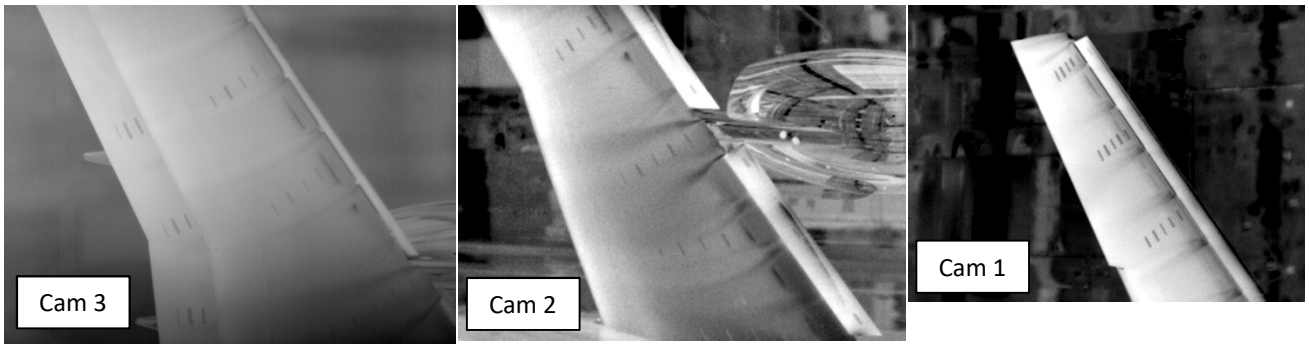

Figure 15 – Infrared images for the NASA CRM-HL configuration for M = 0.2 and α = 18.1° [9]

Extended portion of laminar flow have not been detected in the relevant angle of attack range, but only for angles of attack below -2°. Yet, at α_{max}, laminar separation bubbles have been observed on the slat in the vicinity of the nacelle position, visible by the dark grey color in the Cam 2 picture in Figure 15.

4.6 Aero Acoustic Measurements

Acoustic measurements have been taken in both test section set-ups and for both model variants. According to the respective purpose, the set-up for the measurements differs. For the closed test section, the localization of noise sources is of prime interest. A wall array of 100 GRAS-Microphones of type 48LX-1 UTP with an aperture of 1.6 m × 1.6 m has been used, see Figure 16. The positioning of the microphones on the array has been optimized. Each data point has been recorded with a sampling frequency of 200 kHz for a time period of 30 sec. Both configurations have been measured at M = 0.15, 0.18, 0.20, 0.23 for angles of attack between 1.2° and 7.2° with the high lift devices in takeoff and landing setting. The results have been evaluated with a beamforming method. Details can be found in Ref. [21].

Figure 16 – Microphone wall array mounted on the sidewall of the closed test section [21]

As a preliminary example of the evaluated results, Figure 17 show noise sources of the DLR CRM-HL

configuration. The tracks of the Krueger flaps can be clearly identified as noise sources. The color coding is representative for the different frequencies. A detailed discussion of the acoustic analysis in the closed test section is given in Ref. [21].

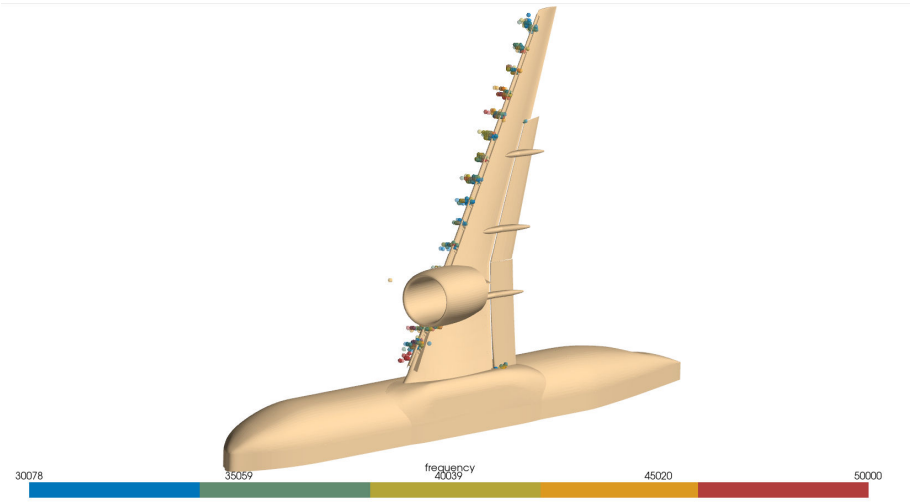

Figure 17 – Assessment of noise sources on the DLR CRM-HL in the closed test section

For the acoustic measurements in the ¾ open test section, a microphone array as well as single microphones have been used as shown in Figure 18.

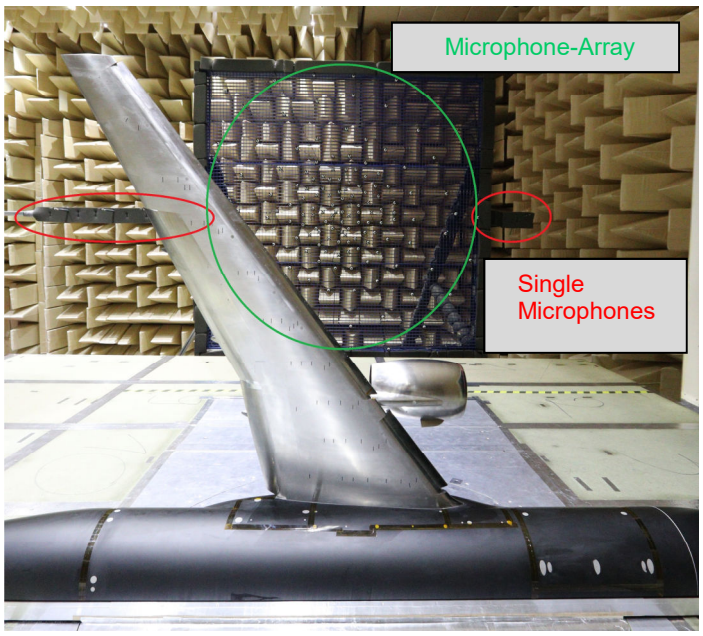

Figure 18 – Microphone set-up for the NASA CRM-HL in the open test section

While the single microphones are recording the overall sound pressure level, a breakdown of the complex source arrangement into components becomes feasible with the microphone array. This allows insight of the impact of specific sources on the measured overall sound pressure level of the single microphones. The related evaluations are ongoing.

5. Conclusion

A test campaign in the DNW-NWB has been carried out by DLR under atmospheric conditions based on the NASA CRM-HL configuration as a contribution to the CRM-HL Ecosystem. The campaign is

split in two blocks with a focus on aerodynamic aspects in the maximum lift regime using the closed test section of the tunnel and a second entry utilizing the open test section, which serves to investigate the impact of the test section scenario, but also to carry out aero-acoustic measurements. In addition to the reference configuration of the NASA CRM-HL model, a configurative variant has been designed and provided by DLR, featuring a vented foldable Krueger flap and a larger UHBR-through flow nacelle with an adapted pylon. Both configurations have been tested in both test section set-ups in landing and take-off configuration.

The aerodynamic tests comprise classical forces and moment measurements and surface pressure distributions on the wing and the nacelle. Transition has been determined on the leading edge devices using infrared thermography. Aerial velocity measurements have been carried out using PIV in longitudinal sections of the flow field. The measurements in the open test section have provided forces and moments, as well as pressure distributions over the whole lift regime up to and including $C_{L,max}$. The acoustic properties are determined by microphone arrays and single microphone measurements. Wall array measurements have also been carried out scheduled in the aerodynamic test in the closed test section. Selected examples of all measurement techniques have been presented and briefly discussed. All in all, a comprehensive dataset has been assembled for low Reynolds number conditions. Cross comparisons to low Reynolds number results with the 5.2% scale NASA CRM-HL model in the NASA NTF reveal a close matching of the forces and moments and the pressure distributions confirming the validity of the test.

While parts of the test results have been evaluated and also published, a lot of test data needs detailed analysis and assessments to be carried out in the future.

6. Acknowledgement

The authors like to acknowledge the support of NASA LaRC for providing the wind tunnel model and personnel to support the model preparation and testing. In addition, the authors would like to thank DLR's model shop SHT and the technical staff of the DNW-NWB for the support during the test campaign.

7. Copyright Statement

References

[1] Rudnik, R., Melber-Wilkending, S., Risley-Settle, P., TAU-SOLAR Contributions to the 3rd High Lift Prediction Workshop, *AIAA Aerospace Science and Technology Forum and Exposition, SciTech 2018*, Kissimmee, FL, 04 - 08 January 2018, AIAA 2018-1035, https://doi.org/10.2514/6.2018-1035, (2018)

[2] Probst, A., Melber-Wilkending, S., Numerical and modeling investigations of the high-lift CRM configuration using hybrid RANS/LES, *AIAA Aviation Forum 2022*, 27.06. – 01.07.2022, Chicago, USA. AIAA 2022-3590, doi: 10.2514/6.2022-3590 <https://doi.org/10.2514/6. (2022).

[3] Probst, A., Melber-Wilkending, s., Hybrid RANS/LES of a generic high-lift aircraft configuration near maximum lift. *International Journal of Numerical Methods for Heat and Fluid Flow*, pp. 1-18. Emerald Group Publishing Ltd.. doi: 10.1108/HFF-08-2021-0525 <https://doi.org/10.1108/HFF-08-2021-0525, ISSN 0961-5539 (2021)

[4] Rumsey, Ch. L., Slotnick, J. P., Sclafani, A.J., Overview and Summary of the Third AIAA High Lift Prediction Workshop*, AIAA Journal of Aircraft*, Volume 56, Number 2, https://doi.org/10.2514/1.C034940, March 2019

[5] Grabe, C., DLR-Project ADaMant: Adaptive, Data-driven Physical Modeling towards Border of Envelope Applications. Presentation at *DLRK 2022. DLRK 2022 Deutscher Luft- und Raumfahrtkongress*, 2022-

09-27 - 2022-09-29, Dresden, Deutschland.

[6] Lacy, D. S., Sclafani, A. J., Development of the High Lift Common Research Model (HL-CRM): A Representative High Lift Configuration for Transonic Transports, *54th AIAA Aerospace Sciences Meeting, 4-8 January 2016*, San Diego, California, USA, AIAA Paper 2016-0308, 2016 https://doi.org/10.2514/6.2016-0308, January 2016.

[7] Lacy. D., Clark, Adam M., Definition of Initial Landing and Takeoff Reference Configurations for the High Lift Common Research Model (CRM-HL), *AIAA AVIATION Forum, June 15-19, 2020*, Virtual Event, 10.2514/6.2020-2771, AIAA Paper 2020-2771, 2020

[8] Evans, A., Lacy, D., Smith, I., Rivers, M., Test Summary of the NASA Semi-Span High-Lift Common Research Model at the QinetiQ 5-Metre Low-Speed Wind Tunnel," *AIAA AVIATION Forum, June 15-19, 2020*, Virtual Event, doi: 10.2514/6.2020-2770, AIAA 2020-2770, 2020.

[9] Pülm, S., Schmidt, F. N., Rudnik, R., Winski, C. S., Low-Speed Testing of the 5.2% Semispan CRM-HL in the DNW-NWB Wind Tunnel, *AIAA Aviation Forum and Ascend 2024, 29 July - 2 August 2024*, Las Vegas, Nevada, https://doi.org/10.2514/6.2024-3516, AIAA paper 2024-3516, 2024

[10] Schmidt, F. N., Wild, J., Design of an UHBR Through Flow Nacelle and a Krueger Flap for the CRM-HL, AIAA SciTech Forum, 8-12 January 2024, Orlando, FL, https://doi.org/10.2514/6.2024-2851, AIAA paper 2024-2851, 2024

[11] Rudolph, P.K.C., High-Lift Systems on Commercial Subsonic Airliners, *NASA-CR-4746*, 1996.

[12] Pott-Pollenske, M., Wild, J., On the Noise Generation of Krueger Leading Edge Devices, 21st *AIAA/CEAS Aeroacoustics Conference*, Dallas, Texas, June 2015., doi: 10.2514/6.2015-3142, AIAA 2015-3142, 2015

[13] Strüber, H., Wild, J., Aerodynamic Design of a High-Lift System Compatible with a Natural Laminar Flow Wing within the DeSiReH Project, *29th Congress of the International Council of the Aeronautical Sciences*, 2014, Paper-ID ICAS 2014-0300.

[14] Wild, J., Palazzo, S., Brinza, I., van der Biest, K., Vervliet, A., Schmitz, H., Design and Testing a Full-Scale Laminar Wing Leading Edge High-Lift System, In: Knoerzer, D., Periaux, J., Tuovinen, T. (eds) *Advances in Computational Methods and Technologies in Aeronautics and Industry. Computational Methods in Applied Sciences*, Vol 57. Springer, Cham, pp. 119–130. doi: 10.1007/978-3-031-12019-0_9, 2022

[15] Spinner, S., Rudnik, R., Design of a UHBR Through Flow Nacelle for High Speed Stall Wind Tunnel Investigations," *Deutscher Luft- und Raumfahrtkongress 2021*, Bremen, 2021., doi: 10.25967/550043

[16] Tejero, F., Goulos, I., MacManus, D., and Sheaf, C., Effects of Aircraft Integration on Compact Nacelle Aerodynamics, *AIAA Scitech Forum*, Orlando, Florida, January 2020. doi: 10.2514/6.2020-2225, AIAA paper 2020-2225, 2020

[17] Subbian, G., Magrini, A., Buosi, D., Radespiel, R. Ponza, R., Benini, E., Investigation of HL-CRM Aerodynamics with a UHBPR Nacelle in Powered-on Condition, *AIAA Propulsion and Energy Forum*, virtual event, 2021, doi: 10.2514/6.2021-3547, AIAA paper 2021-3547, 2021

[18] Spinner, S., and Rudnik, R., Design of a UHBR Through Flow Nacelle for High Speed Stall Wind Tunnel Investigations, *Deutscher Luft- und Raumfahrtkongress* 2021, Bremen, doi: 10.25967/550043, 2021

[19] Bergmann, A., "The Aeroacoustic Wind Tunnel DNW-NWB," *18th AIAA/CEAS Aeroacoustics Conference*, Colorado Springs, Colorado, June 2012. doi: 10.2514/6.2012-2173, AIAA 2012-2173, 2012

[20] Pülm, Sven, Schmidt, Florina, Rudnik, Ralf; Schmidt Moritz, Wolff, Johannes, Low-Speed Testing of Variations of the 5.2% CRM-HL with an UHBR Nacelle and a Krueger Flap in the DNW-NWB Wind Tunnel, accepted for *AIAA Scitech Forum*, Orlando, Florida, January 2025.

[21] Goudarzi, A., Ahlefeldt, T., Ernst, D., Spehr, C., Aeroacoustic evaluation of the NASA High-Lift Common Research Model model with standard and DLR Krüger slat configuration, *30th AIAA/CEAS Aeroacoustics Conference*, June 4-7, 2024, Rome, Italy, https://doi.org/10.2514/6.2024-3169, AIAA paper 2024-3169, 2024

[22] Raffel M, Willert CE, Scarano F, Kähler CJ, Wereley ST, Kompenhans J., Particle Image Velocimetry: A Practical Guide. 3rd Edition, *Springer Verlag*, ISBN: 978-3-319-68851-0, DOI: 10.1007/978-3-319-68852-7, 2018

[23] Rumsey, Ch. L., Slotnick, J. P., and Woeber, C. D., "HLPW-4/GMGW-3: Overview and Workshop Summary," *AIAA Aviation Forum*, Chicago, Illinois, June-July 2022. doi: 10.2514/6.2022-3295, AIAA 2022-3295, 2022